Scientific Research Publishing

American Journal of Computational Mathematics, 2022, 12, 267-282
https://www.scirp.org/journal/ajcm
ISSN Online: 2161-1211
ISSN Print: 2161-1203

Insight into Dynamics of Hydromagnetic Flow of Micropolar Fluid Containing Nanoparticles and Gyrotactic Microorganisms at Weak and Strong Concentrations of Microelements: Homotopy Analysis Method

Olubode Kolade Koriko[1], Adeola John Omowaye[1], Amos Oladele Popoola[2], Tosin Oreyeni[3*], Abigail Ayooye Adegbite[3], Emmanuel Abiodun Oni[4], Emmanuel Omokhuale[5], Muhammad Muhammad Altine[6]

[1]Department of Mathematical Sciences, Federal University of Technology Akure, Akure, Nigeria
[2]Department of Mathematical Sciences, Osun State University, Osogbo, Nigeria
[3]Department of Physical Sciences, Precious Cornerstone University, Ibadan, Nigeria
[4]Department of Pure and Applied Physics, Ladoke Akintola University of Technology, Ogbomosho, Nigeria
[5]Department of Mathematical Sciences, Federal University Gusau, Gusau, Nigeria
[6]Department of Mathematics, Federal University Birnin Kebbi, Kalgo, Nigeria
Email: okkoriko@futa.edu.ng, ajomowaye@futa.edu.ng, amos.popoola@uniosun.edu.ng, *oreyenitos@gmail.com, ayooye24@yahoo.com, emand1215@gmail.com, emmanuelomokhuale@yahoo.com, altine@fubk.edu.ng

How to cite this paper: Koriko, O.K., Omowaye, A.J., Popoola, A.O., Oreyeni, T., Adegbite, A.A., Oni, E.A., Omokhuale, E. and Altine, M.M. (2022) Insight into Dynamics of Hydromagnetic Flow of Micropolar Fluid Containing Nanoparticles and Gyrotactic Microorganisms at Weak and Strong Concentrations of Microelements: Homotopy Analysis Method. *American Journal of Computational Mathematics*, **12**, 267-282.
https://doi.org/10.4236/ajcm.2022.122017

Received: July 30, 2021
Accepted: June 25, 2022
Published: June 28, 2022

Abstract

The mathematical model of bioconvection flow of micropolar fluid through a vertical surface containing nanoparticles and gyrotactic microorganisms is presented in this study. In the study, weak and strong concentrations of microstructures are explored. In the energy and concentration equations, the Catteneo-Christov diffusion models are used to explain temperature and concentration diffusions with thermal and solutal relaxation durations, respectively. The governing equations describing the fluid flow are transformed and parameterized through similarity variables. The approximate analytical solution is obtained by using Homotopy Analysis Method (HAM). The impacts of relevant parameters on the various distributions are investigated and illustrated. It is discovered that increasing the value of the micropolar parameter results in an increase in the microrotation distribution for strong concentrations of microstructures while decreasing the microrotation distribution for weak concentrations of microstructures.

Keywords

Micropolar Fluid, Bioconvection, Gyrotactic Microorganisms, Nanofluid,

Homotopy Analysis Method

1. Introduction

Bioconvection is the phenomenon of pattern creation found in the aqueous solution of motile microorganisms when they respond to specific stimuli by swimming in certain directions named taxes Platt [1]. According to Ghorai and Hill [2], gyrotaxis is swimming driven by the balance of torque due to gravity acting on a bottom-heavy cell and torque owing to viscous forces resulting from local shear flows. According to the study of Raees *et al.* [3], bioconvection in nanofluids holds great potential in the Colibri micro-volumes spectrometer as well as in improving the stability of nanofluids. They also showed the application of bioconvection in the field of microbial enhanced oil recovery, which involves injecting selected microorganisms into the reservoir and multiplying them in situ to reduce the residual oil left in the reservoir once secondary recovery is exhausted. Waqas *et al.* [4] discussed the effects of activation energy and thermal radiation in the bioconvection flow of third-grade nanofluid. Ramzan *et al.* [5] presented bioconvective Reiner-Rivlin nanofuid flow over a rotating disk. It was reported that motile density distribution diminishes for large values of bioconvective Lewis numbers. Manjunatha *et al.* [6] explicated quartic autocatalysis of homogeneous and heterogeneous reactions in the bioconvective flow of radiating micropolar nanofluid. Koriko *et al.* [7] exploited active and passive controls of bioconvection flow of thixotropic fluid with Catteno-Christov phenomenon. They reported that density of motile microorganisms profile diminish for stronger values of bioconvective parameter for both active and passive controls of nanoparticles. MHD bioconvection flow of Casson nanofluid over a rotating disk was explored by Jawad *et al.* [8]. It was reported that density of motile gyrotactic microorganisms distribution declines with larger values of bioconvection Peclet number.

For many years, the dynamics of fluid with small particles has been a major topic of research in industry. It is a well-known fact that each particle in this type of fluid typically rotates independently of the fluid's velocity. Micropolar fluids are viscous fluids composed of rigid, randomly oriented particles suspended in a viscous liquid. Eringen [9] proposed the concept of micropolar fluid in an attempt to characterize the behavior of a specific fluid including polymeric additives and naturally occurring fluids such as colloidal fluid flow, liquid crystals, and animal blood. Heat and mass transfer of MHD micropolar fluid flow along a permeable channel was examined by Agarwal *et al.* [10]. Shamshuddin *et al.* [11] studied characteristics of thermophoresis and Brownian motion on radiative reactive micropolar fluid flow towards continuously moving flat plate. Numerical simulation of stagnation point flow in magneto micropolar fluid over a stretchable surface under influence of activation energy and bilaterial reaction was explored by Shamshuddin *et al.* [12]. Influence of viscous dissipation on MHD

flow of micropolar fluid over a slendering stretching surface with modified heat flux model was presented by Kumar *et al.* [13]. Kumar *et al.* [14] considered physical aspects on unsteady MHD free convective stagnation point flow of micropolar fluid over a stretching surface. Koriko *et al.* [15] analysed boundary layer flow of micropolar fluid with combined nonlinear thermal radiation and thermal stratification. They observed that when there is a high concentration of microstructures, the rate of rise in vertical velocity is faster than when there is a low concentration of microstructures. Homotopy analysis of MHD free convection flow of micropolar fluid subjected stratified environment was examined by Koriko *et al.* [16].

Heat transfer has become an essential component of all industrial activities. As a result, it must be added, removed, or moved from one phase to the next. Heat transfer efficiency may be improved by increasing the thermal conductivity of the working fluid. Choi and Eastman [17] pioneered the concept of heat transfer enhancement when they developed an efficient approach to adjust heat transfer rate utilizing nanoparticles in their experiment. Nanofluids are employed in a wide range of engineering applications because of their enhanced heat transfer efficiency in diverse thermal systems. Nanofluids may find applications in engine coolant, automatic transmission fluid, brake fluid, gear lubrication, engine oil, and greases Senthilraja *et al.* [18]. Shah *et al.* [19] scrutinized analytic solution of Brownian motion and thermophoretic diffusion effects on Maxwell fluid containing tiny particles. It was reported that both the velocity and temperature distributes are enhanced for larger Brownian motion and thermophoretic parameter. Amar and Kishan [20] examined radiation effects on Mhd boundary layer flow of a nanofluid. Mhd stagnation point flow of a nanofluid with solar radiation effects was studied by Ghasemi and Hatami [21]. Rasool and Zhang [22] considered characteristics of chemical reaction and convective boundary conditions in Powell-Eyring nanoflid flow along a radiative Riga plate. It was reported that Brownian motion factor and thermophoresis improve the thermal boundary layer. Fayyadh *et al.* [23] discussed the influence of Biot number on the convective heat transfer of Darcy-Forchheimer nanofluid flow over stretched zero mass flux surface in the presence of magnetic field. Nayak *et al.* [24] examined partial slip and viscous dissipation effects on the radiative tangent hyperbolic nanofluid flow via a vertical permeable riga plate with internal heating. It was reported that the concentration of nanoparticles increases for larger thermophoretic force in the flow domain owing to the dragging process.

Motivated by all of the research on non-Newtonian fluid boundary layer flow past a vertical surface. The aim of this work is to investigate the bioconvection flow of micropolar fluid containing nanoparticles and gyrotactic microorganisms, with Catteneo-Christov model at the instances of strong and weak concentrations of microelements.

2. Mathematical Formulation

In accordance with boundary layer theory, a steady, buoyant convective boun-

dary layer equation of micropolar nanofluid is investigated to achieve our goals. The flow is considered to be in the x-direction, which runs vertically along the plate, with y-direction being normal to it. Nanoparticles are considered to have little effect on the direction and speed with which microorganisms swim. Bioconvection flow is thought to occur exclusively in dilute nanoparticle suspensions. It is important to note that the base fluid is water in order for the microorganisms to survive. Under the foregoing assumptions with Boussinesq approximation and following the works of Koriko *et al.* [15], Koriko *et al.* [16], Hayat *et al.* [25] and Saleem *et al.* [26] the governing equations for mass, momentum, energy, and density of gyrotactic microorganisms in two-dimensional micropolar nanofluid may be expressed as follows;

Continuity Equation

$$\frac{\partial u}{\partial x}+\frac{\partial v}{\partial y}=0, \tag{1}$$

Momentum Equation

$$\begin{aligned} u\frac{\partial u}{\partial x}+v\frac{\partial u}{\partial y}&=\left(\frac{\mu+\chi}{\rho_f}\right)\frac{\partial^2 u}{\partial y^2}+\frac{\chi}{\rho_f}\frac{\partial H}{\partial y}-\sigma\frac{B_o^2 u}{\rho_f}\\ &+\frac{(1-C_\infty)\rho_f g\beta(T-T_\infty)-g(\rho_p-\rho_f)(C-C_\infty)-g\gamma(\rho_m-\rho_f)(N-N_\infty)}{\rho_f}, \end{aligned} \tag{2}$$

Angular Momentum Equation

$$u\frac{\partial H}{\partial x}+v\frac{\partial H}{\partial y}=\left(\frac{\mu+\chi/2}{\rho j}\right)\frac{\partial^2 H}{\partial y^2}-\frac{\chi}{\rho j}\left(2H+\frac{\partial u}{\partial y}\right), \tag{3}$$

Energy equation of nanoparticles

$$\begin{aligned} u\frac{\partial T}{\partial x}+v\frac{\partial T}{\partial y}&=\frac{\kappa}{\rho C_p}\frac{\partial^2 T}{\partial y^2}+\tau\left(D_B\frac{\partial T}{\partial y}\frac{\partial C}{\partial y}+\frac{D_T}{T_\infty}\left(\frac{\partial T}{\partial y}\right)^2\right)\\ &+\lambda_1\left(u^2\frac{\partial^2 T}{\partial x^2}+v^2\frac{\partial^2 T}{\partial y^2}+2uv\frac{\partial^2 T}{\partial y\partial x}+u\frac{\partial u}{\partial x}\frac{\partial T}{\partial x}+u\frac{\partial v}{\partial x}\frac{\partial T}{\partial y}+v\frac{\partial u}{\partial y}\frac{\partial T}{\partial x}+v\frac{\partial v}{\partial y}\frac{\partial T}{\partial y}\right), \end{aligned} \tag{4}$$

Concentration equation of nanoparticles

$$\begin{aligned} u\frac{\partial C}{\partial x}+v\frac{\partial C}{\partial y}&=D_B\frac{\partial^2 C}{\partial y^2}+\frac{D_T}{T_\infty}\frac{\partial^2 T}{\partial y^2}\\ &+\lambda_2\left(u^2\frac{\partial^2 C}{\partial x^2}+v^2\frac{\partial^2 C}{\partial y^2}+2uv\frac{\partial^2 C}{\partial y\partial x}+u\frac{\partial u}{\partial x}\frac{\partial C}{\partial x}+u\frac{\partial v}{\partial x}\frac{\partial C}{\partial y}+v\frac{\partial u}{\partial y}\frac{\partial C}{\partial x}+v\frac{\partial v}{\partial y}\frac{\partial C}{\partial y}\right), \end{aligned} \tag{5}$$

Density of gyrotactic microorganisms equation

$$u\frac{\partial N}{\partial x}+v\frac{\partial N}{\partial y}+\frac{bW_c}{C_w-C_\infty}\left[\frac{\partial}{\partial y}\left(N\frac{\partial C}{\partial y}\right)\right]=D_m\frac{\partial^2 N}{\partial y^2} \tag{6}$$

The equations above are subjected to the following boundary conditions:

$$u=ax,\ v=0,\ H=-n\frac{\partial u}{\partial y},\ T=T_w,\ C=C_w,\ N=N_w\ \text{ at }\ y=0, \tag{7}$$

$$u\to 0,\ H\to 0,\ T\to T_\infty,\ C\to C_\infty,\ N\to N_\infty\ \text{ as }\ y\to\infty \tag{8}$$

where u and v are velocity components in x and y directions respectively, c_h is the chemotaxis constant, W_c is the maximum cell swimming speed, m is the velocity power index, T_f is the local fluid, T is the temperature of the fluid, C is the nanoparticle, N is the density of motile micro-organisms, p is the pressure, ρ_f, ρ_p, ρ_m are the density of nanofluid, nanoparticles and micro-organisms respectively, D_B, D_T, D_m are the Brownian diffusion coefficient, thermophoresis diffusion coefficient and diffusivity of micro-organisms respectively, κ, σ are the thermal and electrical conductivity of the fluid respectively, α is the thermal diffusivities, τ is the ratio of the effective heat capacitance of the nanoparticle to that of the base fluid, j is the micro-inertial density, χ is the vortex viscosity, n is the surface condition parameter and varies from 0 to 1. The study considers two cases when $n=0$ and $n=1/2$. When $n=0$ (called strong concentration) indicates concentrated particle flows in which the microelements close to the wall are unable to spin, $H=0$ near the wall and H is the micro-rotation or angular velocity whose direction of rotation is in the xy plane. When $n=1/2$, the anti-symmetric component of the stress tensor vanishes, indicating a weak concentration of microelements, when $n=1$, the situation is utilized for simulating turbulent boundary layer flows. The micropolar parameter, often known as the material parameter, is $K=\frac{\chi}{\mu}$, $K\neq 0$ for micropolar fluid and $K=0$ for classical Newtonian fluid.

For the sake of non-dimensionalization and parameterization of Equations (2)-(5) and (6) subject to boundary conditions (7) and (8), the following similarity variables are considered corresponding to the following models:

$$\begin{aligned} &\eta=\frac{a^{\frac{1}{2}}}{\vartheta^{\frac{1}{2}}}y, \quad \frac{\psi(x,y)}{xa^{\frac{1}{2}}\vartheta^{\frac{1}{2}}}=f(\eta), \quad H=ax\left(\frac{a}{\vartheta}\right)^{1/2}, \\ &\theta(\eta)=\frac{T-T_\infty}{T_w-T_\infty}, \quad \phi=\frac{C-C_\infty}{C_w-C_\infty}, \quad w(\eta)=\frac{N-N_\infty}{N_w-N_\infty}, \end{aligned} \tag{9}$$

when the stream function $\psi(x,y)$ is introduced the continuity Equation (1) is automatically satisfied then Equations (2)-(6) become

$$(1+K)\frac{\mathrm{d}^3 f}{\mathrm{d}\eta^3}-\left(\frac{\mathrm{d}f}{\mathrm{d}\eta}\right)^2+f\frac{\mathrm{d}^2 f}{\mathrm{d}\eta^2}+K\frac{\mathrm{d}p}{\mathrm{d}\eta}-M\frac{\mathrm{d}f}{\mathrm{d}\eta}+G_r\theta-N_r\phi+R_b w \tag{10}$$

$$\left(1+\frac{K}{2}\right)\frac{\mathrm{d}^2 p}{\mathrm{d}\eta^2}+f\frac{\mathrm{d}p}{\mathrm{d}\eta}-p\frac{\mathrm{d}f}{\mathrm{d}\eta}-K\left(2p+\frac{\mathrm{d}^2 f}{\mathrm{d}\eta^2}\right)=0 \tag{11}$$

$$\frac{\mathrm{d}^2\theta}{\mathrm{d}\eta^2}+P_r f\frac{\mathrm{d}\theta}{\mathrm{d}\eta}-P_r\delta_t\left(f^2\frac{\mathrm{d}^2\theta}{\mathrm{d}\eta^2}+f\frac{\mathrm{d}f}{\mathrm{d}\eta}\frac{\mathrm{d}\theta}{\mathrm{d}\eta}\right)+P_r N_b\frac{\mathrm{d}\phi}{\mathrm{d}\eta}\frac{\mathrm{d}\theta}{\mathrm{d}\eta}+P_r N_t\left(\frac{\mathrm{d}\theta}{\mathrm{d}\eta}\right)^2=0 \tag{12}$$

$$\frac{\mathrm{d}^2\phi}{\mathrm{d}\eta^2}+L_e f\frac{\mathrm{d}\phi}{\mathrm{d}\eta}-L_e\delta_n\left(f^2\frac{\mathrm{d}^2\phi}{\mathrm{d}\eta^2}+f\frac{\mathrm{d}f}{\mathrm{d}\eta}\frac{\mathrm{d}\phi}{\mathrm{d}\eta}\right)+\frac{N_t}{N_b}\frac{\mathrm{d}^2\theta}{\mathrm{d}\eta^2}=0 \tag{13}$$

$$\frac{\mathrm{d}^2 w}{\mathrm{d}\eta^2}+S_{cm}f\frac{\mathrm{d}w}{\mathrm{d}\eta}-P_e\varsigma\frac{\mathrm{d}^2\phi}{\mathrm{d}\eta^2}-P_e w\frac{\mathrm{d}^2\phi}{\mathrm{d}\eta^2}-P_e\frac{\mathrm{d}\phi}{\mathrm{d}\eta}\frac{\mathrm{d}w}{\mathrm{d}\eta}=0 \tag{14}$$

subject to the boundary conditions (7) and (8) which becomes;

$$f(0)=0,\ \frac{\mathrm{d}f(0)}{\mathrm{d}\eta}=1,\ p(0)=-n\frac{\mathrm{d}^2 f}{\mathrm{d}\eta^2},\ \theta(0)=1,\ \phi(0)=1,\ w(0)=1, \quad (15)$$

$$\frac{\mathrm{d}f(\infty)}{\mathrm{d}\eta}=0,\ p(\infty)=0,\ \theta(\infty)=0,\ \phi(\infty)=0,\ w(\infty)=0 \quad (16)$$

In the above equations primes denote differentiation with respect to η. The dimensionless velocity, temperature, concentration and density of microorganisms are represented as $f(\eta)$, $p(\eta)$, $\theta(\eta)$, $\phi(\eta)$ and $w(\eta)$. $P_r=\frac{\vartheta}{\alpha}$ is the Prandtl number, $M=\sigma\frac{B_o^2}{\rho_f a}$ is the magnetic parameter,

$G_r=\frac{g\rho_{f_\infty}\beta(1-C_\infty)(T_f-T_\infty)}{\rho_f a^2 x}$ is the modified local Grashof number,

$N_r=\frac{g(C_w-C_\infty)(p_\rho-p_f)}{\rho_f a^2 x}$ is the buoyancy-ratio parameter,

$R_b=\frac{g\gamma(C_w-C_\infty)(N-N_\infty)}{\rho_f a^2 x}$ is the bioconvection Rayleigh number,

$N_b=\frac{(\rho C)_p}{\vartheta(\rho C)_f}D_B(C_w-C_\infty)$ is the Brownian motion parameter,

$N_t=\frac{(\rho C)_p}{\vartheta(\rho C)_f}\frac{D_T}{T_\infty}(T_w-T_\infty)$ is the thermophoresis parameter, $\delta_t=\lambda_1 a$ is the relaxation time parameter of temperature, $L_e=\frac{\vartheta}{D_B}$ is the Lewis number, $\delta_n=\lambda_2 a$ is the relaxation time parameter of nanoparticle volume fraction, $\varsigma=\frac{N_\infty}{N_w-N_\infty}$ is gyrotactic microorganisms concentration difference parameter, $S_{cm}=\frac{\vartheta}{D_B}$ is the Schmidth number for diffusing motile microorganisms and $P_e=\frac{bW_c}{D_n}$ is the Peclet number.

The dimensionless form of skin friction coefficient,

$$Re^{1/2}C_{fx}=f''(0) \quad (17)$$

The dimensionless form of wall motile microorganisms number,

$$Re^{1/2}Q_{nx}=-w'(0) \quad (18)$$

where $Re=\frac{ax^2}{\vartheta}$ is the local Reynolds number.

3. Homotopy Analysis Method (HAM)

HAM provides a great freedom to express solutions of a given non-linear problem by means of different base functions. Non-linear problems can be approx-

imated more efficiently by choosing a proper set of base functions, mainly because, the convergence region and rate of a series are determined by the base functions used to express the solution [27] [28] [29] [30] [31]. In view of the boundary conditions (15) & (16), $f(\eta)$, $p(\eta)$, $\theta(\eta)$, $\phi(\eta)$ and $w(\eta)$ can be expressed by the set of base functions in the form

$$\left\langle \eta^j \exp(-nj) \mid j \geq 0, n \geq 0 \right\rangle \tag{19}$$

The solutions $f(\eta)$ and $\theta(\eta)$ can be represented in a series form as

$$f(\eta) = a_{0,0}^0 + \sum_{n=0}^{\infty}\sum_{k=0}^{\infty} a_{n,k}^k \eta^k \exp(-nj) \tag{20}$$

$$p(\eta) = \sum_{n=0}^{\infty}\sum_{k=0}^{\infty} b_{n,k}^k \eta^k \exp(-nj) \tag{21}$$

$$\theta(\eta) = \sum_{n=0}^{\infty}\sum_{k=0}^{\infty} c_{n,k}^k \eta^k \exp(-nj) \tag{22}$$

$$\phi(\eta) = \sum_{n=0}^{\infty}\sum_{k=0}^{\infty} d_{n,k}^k \eta^k \exp(-nj) \tag{23}$$

$$w(\eta) = \sum_{n=0}^{\infty}\sum_{k=0}^{\infty} e_{n,k}^k \eta^k \exp(-nj) \tag{24}$$

in which $a_{n,k}^k$, $b_{n,k}^k$, $c_{n,k}^k$, $d_{n,k}^k$ and $e_{n,k}^k$ are the coefficients. As long as such a set of base functions are determined, the auxiliary function $H(\eta)$, the initial approximation $f_o(\eta), p_o(\eta), \theta_o(\eta), \phi_o(\eta)$ and $w_o(\eta)$ and the auxiliary linear operator $L_f, L_p, L_\theta, L_\phi$ and L_w must be chosen in such a way that all solutions exist and can be expressed by these sets of base functions. Therefore, in framing the Homotopy Analysis Method (HAM), we apply the rule of solution expressions in choosing the auxilliary function $H(\eta)$, initial approximation $f_o(\eta), p_o(\eta), \theta_o(\eta), \phi_o(\eta)$ and $w_o(\eta)$.

Invoking the rule of solution expressions for $f(\eta), p(\eta), \theta(\eta), \phi(\eta)$ and $w(\eta)$ for Equations (15) & (17) together with (18)-(21) are expressed as

$$\begin{aligned} &f_o(\eta) = 1 - \exp(-\eta), \quad p_o(\eta) = -n * \exp(-\eta), \quad \theta_o(\eta) = \exp(-\eta), \\ &\phi_o(\eta) = \exp(-\eta), \quad w_o(\eta) = \exp(-\eta) \end{aligned} \tag{25}$$

with linear operators L_f, L_θ, L_ϕ and L_w as

$$L_f\left[f(\eta;q)\right] = \frac{\partial^3 f(\eta;q)}{\partial \eta^3} - \frac{\partial f(\eta;q)}{\partial \eta} \tag{26}$$

$$L_p\left[p(\eta;q)\right] = \frac{\partial^2 p(\eta;q)}{\partial \eta^2} - p(\eta;q) \tag{27}$$

$$L_\theta\left[\theta(\eta;q)\right] = \frac{\partial^2 \theta(\eta;q)}{\partial \eta^2} - \theta(\eta;q) \tag{28}$$

$$L_\phi\left[\phi(\eta;q)\right] = \frac{\partial^2 \phi(\eta;q)}{\partial \eta^2} - \phi(\eta;q) \tag{29}$$

$$L_w\left[w(\eta;q)\right] = \frac{\partial^2 w(\eta;q)}{\partial \eta^2} - w(\eta;q) \tag{30}$$

The linear operators $L_f, L_p, L_\theta, L_\phi$ and L_w have the following properties

$$\begin{aligned} L_f\left[C_1 + C_2\exp(-\eta) + C_3\exp(\eta)\right] &= 0, \\ L_p\left[C_4\exp(-\eta) + C_5\right] &= 0, \\ L_\theta\left[C_6\exp(-\eta) + C_7\right] &= 0, \\ L_\phi\left[C_8\exp(-\eta) + C_9\right] &= 0, \\ L_w\left[C_{10}\exp(-\eta) + C_{11}\right] &= 0 \end{aligned} \tag{31}$$

in which $C_1, C_2, C_3, C_4, C_5, C_6, C_7, C_8, C_9, C_{10}$, and C_{11} are constants.

4. Results and Discussion

The flow of micropolar fluid in a water-based solution containing both nanoparticles and gyrotactic microorganisms has been analyzed for various values of emerging parameters. The effects of various parameters on velocity $f'(\eta)$, microrotation $p(\eta)$, temperature $\theta(\eta)$, nanoparticles concentration $\phi(\eta)$, and motile microorganism density profiles $w(\eta)$ have been studied and reported. The theoretical values of the governing parameters for both cases of weak and strong concentration of microelements are $M = G_r = N_r = R_b = 0.5$, $\delta_t = \delta_n = N_b = N_t = \varsigma = 0.1$, $S_c = P_e = 1.0$, $P_r = 1.2$, $K = 0.4$, $L_e = 2.0$. Table 1 displays the numerical values of the local skin friction coefficient, plate couple stress, local Nusselt number, local Sherwood number, and local density number for different values of the Micropolar parameter *K*, while the other parameters are held constant at strong microstructure concentrations. The local skin friction coefficient is found to be a decreasing function of *K*, with the first two values increasing plate couple stress and the final two entries lowering plate couple stress. The first two *K* entries show an increase in the local Nusselt number, whereas the latter two show a reduction. The local Nusselt number is a decreasing function of *K*, and the first two entries of *K* improve the local density number, while the latter two entries of *K* slightly improve it.

Table 2 displays the numerical values of the local skin friction coefficient, plate couple stress, local Nusselt number, local Sherwood number an local density number for various values of Micropolar parameter *K* when the other parameters are held constant at low microstructure concentrations. The first two *K* values indicate a decrease in the local skin friction coefficient, whereas the latter two entries indicate an increase in the local skin friction coefficient. The first and last two entries of *K* represent an increase and decrease in plate couple stress respectively. It is also worth noting that the local Nusselt number and Sherwood number are both decreasing functions of *K*, whereas the first two and final two entries of *K* cause an increase in the local density number. Figures 1(a)-5(b) show the effect of micropolar parameter *K* on various profiles when $n = 0 \& 0.5$. Figure 1(a) and Figure 1(b) show that the velocity profiles increase as the magnitude of the micropolar parameter *K* augment when $n = 0 \& 0.5$. In Figure 2(a) it is noticed that larger values of micropolar parameter *K* correspond to an increase in the microrotation profile when $n = 0$. It is also demonstrated that the

Table 1. Values of $-f''(0), -p'(0), -\theta'(0), -\phi'(0)$ and $-w'(0)$ for various values K when $M = G_r = R_b = N_r = 0.5$, $N_b = N_t = \varsigma = \delta_t = \delta_n = 0.1$, $P_r = S_{cm} = 1.0$ and $L_e = 2.0$ at the strong concentration of microstructure.

K	$-f''(0)$	$-p'(0)$	$-\theta'(0)$	$-\phi'(0)$	$-w'(0)$
0.1	0.9480	0.8488	1.0780	0.5965	1.0326
0.3	0.6189	0.8559	1.0872	0.5404	1.0991
0.5	0.6079	0.7276	1.0688	0.4784	1.0863
0.7	0.6023	0.6170	1.0493	0.4236	1.0865

Table 2. Values of $-f''(0), -p'(0), -\theta'(0), -\phi'(0)$ and $-w'(0)$ for various values K when $M = G_r = R_b = N_r = 0.5$, $N_b = N_t = \varsigma = \delta_t = \delta_n = 0.1$, $P_r = S_{cm} = 1.0$ and $L_e = 2.0$ at the weak concentration of microstructure.

K	$-f''(0)$	$-p'(0)$	$-\theta'(0)$	$-\phi'(0)$	$-w'(0)$
0.1	0.9650	0.9229	1.0784	0.5915	1.0292
0.3	0.6493	0.9249	1.0738	0.4835	1.0847
0.5	0.6779	0.7596	1.0265	0.3790	1.0547
0.7	0.6845	0.6509	0.9820	0.2935	1.0577

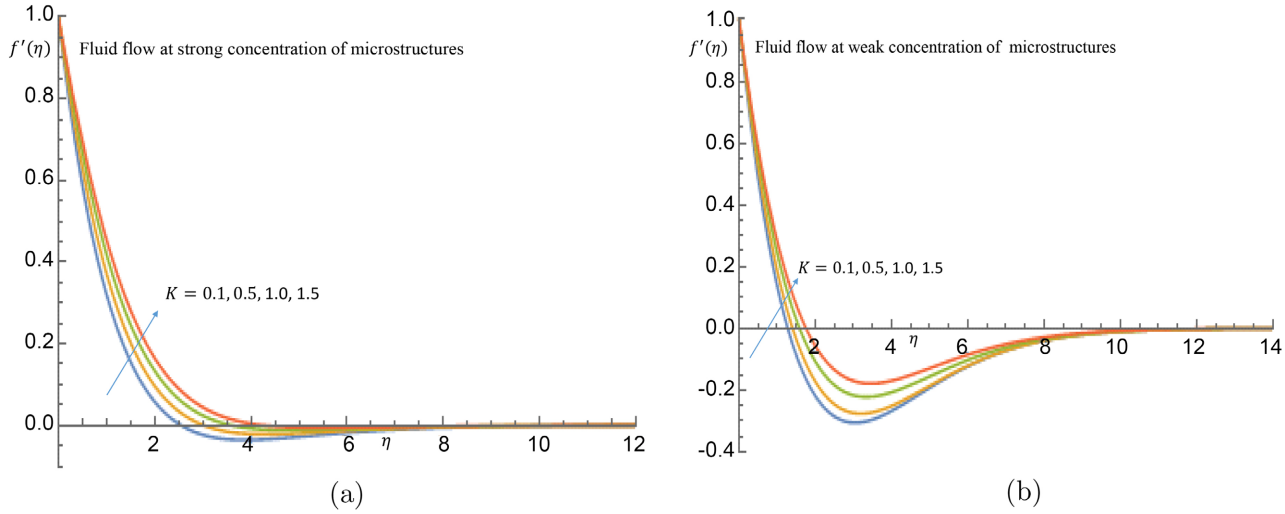

Figure 1. (a) Effect of K on velocity profile when $n = 0$; (b) effect of K on velocity profile when $n = 0.5$.

particle near the wall does not rotate because $n = 0$ depicts concentrated particle flows in which micro-elements close to the wall are unable to rotate.

However as shown in **Figure 2(b)** when the micropolar parameter K grows, the microrotation profile diminishes. **Figure 3(a)** indicates that increasing the value of K yields a reduction in the temperature distribution when $n = 0$ but **Figure 3(b)** shows a more massive decrease in the temperature distribution as the value of K increases. **Figure 4(a)** shows that increasing values of K leads to decrease in the concentration of nanoparticles distribution when $n = 0$ whereas increasing K results in increase in the concentration of nanoparticles within

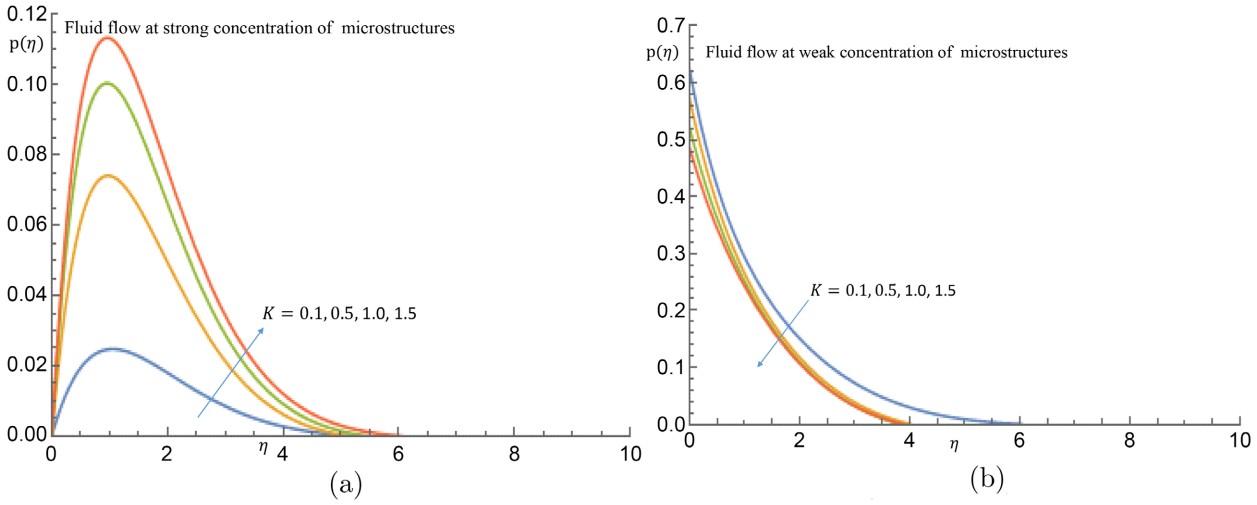

Figure 2. (a) Effect of K on microrotation profile when $n = 0$; (b) effect of K on microrotation profile when $n = 0.5$.

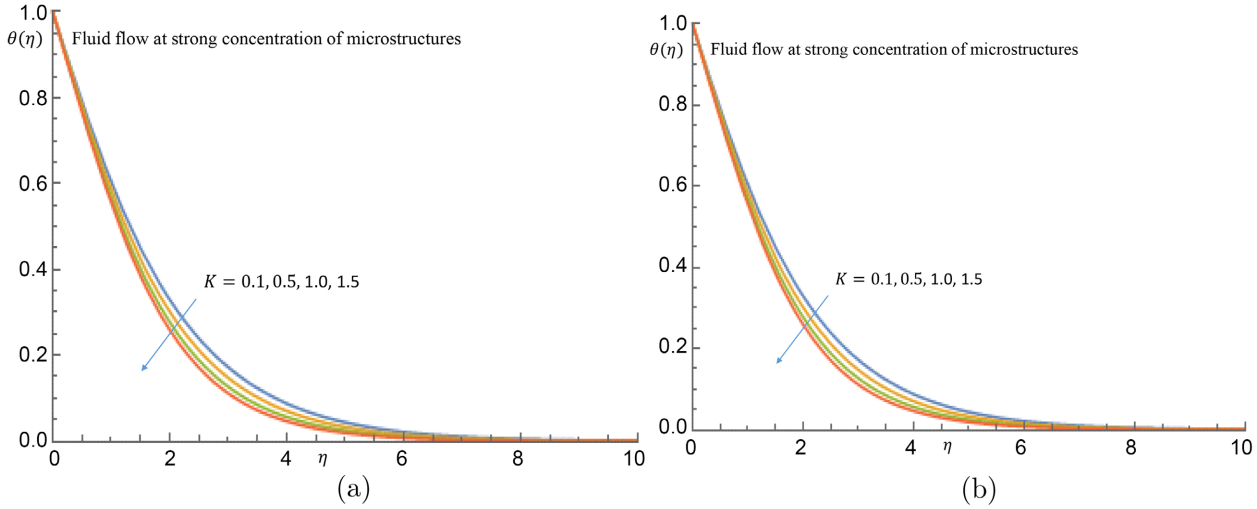

Figure 3. (a) Effect of K on temperature profile when $n = 0$; (b) effect of K on temperature profile when $n = 0.5$.

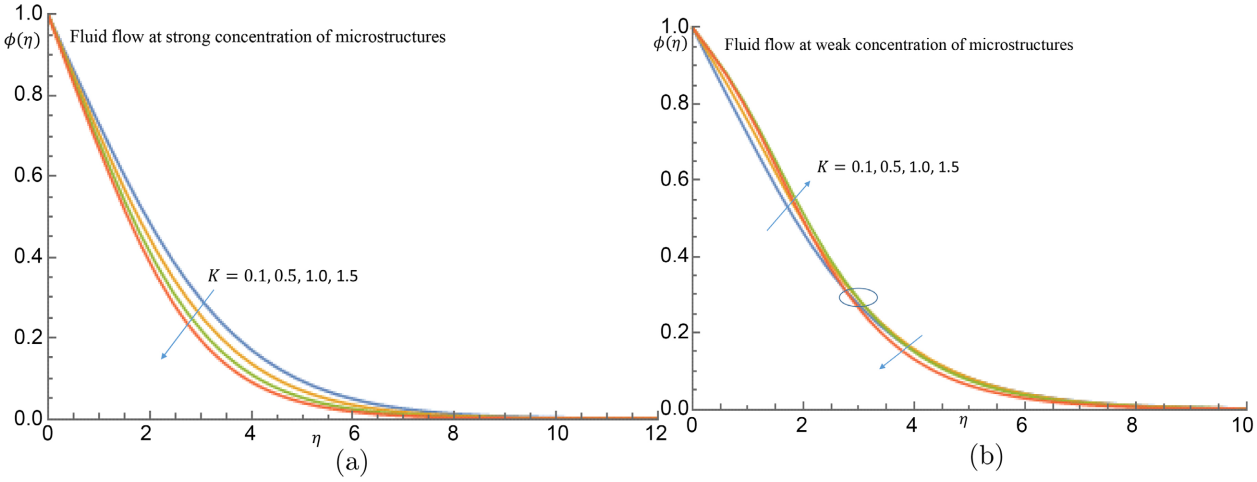

Figure 4. (a) Effect of K on concentration of nanoparticles profile when $n = 0$; (b) effect of K on concentration of nanoparticles profile when $n = 0.5$.

the domain $0 \le \eta \le 2.56$ and thereafter all profiles merged together and later decline towards the freestream. **Figure 5(a)** and **Figure 5(b)** depict the influence of K on the density of motile microorganisms profiles when $n = 0$ and $n = 0.5$. **Figure 5(a)** indicates that increasing K results in a slight decline in the density of motile microorganisms profiles when $n = 0$ but increases the density of motile microorganisms when $n = 0.5$ as revealed in **Figure 5(b)**. The observation in **Figure 5(b)** is completely different from that of **Figure 5(a)** mainly because microorganisms are free to rotate at the wall allowing the profiles to enhance particularly at the bottom layer of the wall.

Figure 6(a) and **Figure 6(b)** depict the effects of M on the microrotation profiles when $n = 0$ and $n = 0.5$ respectively. In **Figure 6(a)** it noticed that when $n = 0$ all profiles fused together at the peak 0.26 and afterwards fall for larger values of M towards the freestream, whereas in **Figure 6(b)** it is observed that there is a conspicuous augmentation in microrotation profile when $n = 0.5$ as M increases.

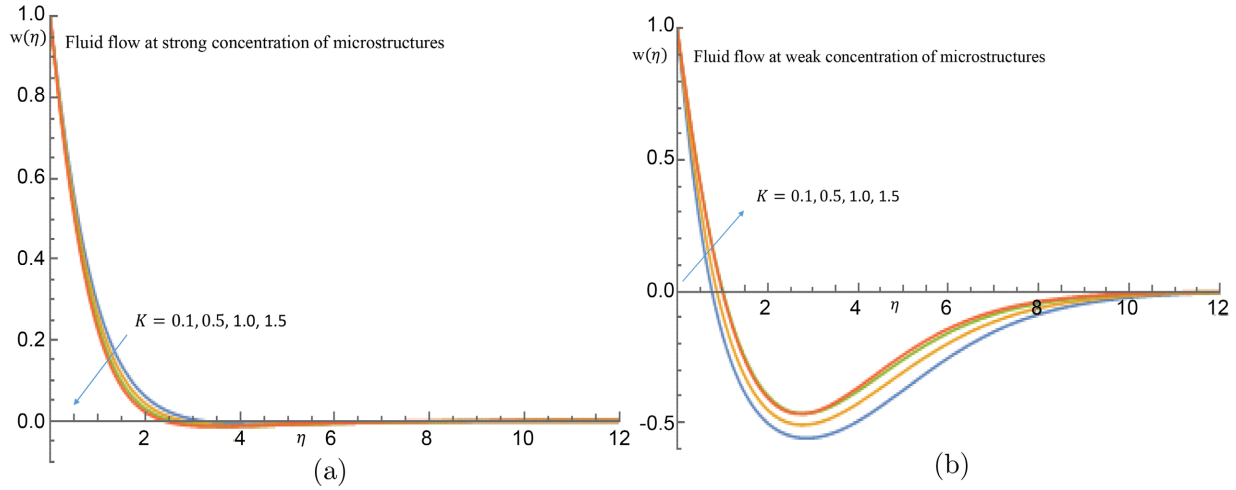

Figure 5. (a) Effect of K on density of motile microorganisms profile when $n = 0$; (b) effect of K on density of motile microorganisms profile when $n = 0.5$.

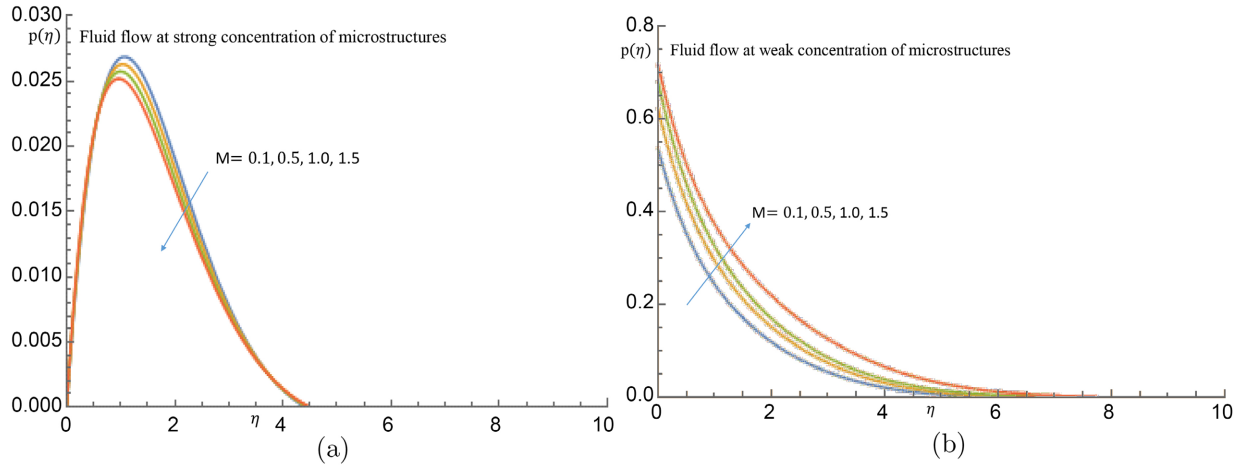

Figure 6. (a) Effect of M on microrotation profile when $n = 0$; (b) effect of M on microrotation profile when $n = 0.5$.

In **Figure 7(a)** when $n=0$ it is revealed that raising the value of N_t produces an increase in the microrotation distribution along the wall. Furthermore, all profiles merged at $\eta=1.6$, resulting in decrease in the microrotation profile. **Figure 7(b)** shows that when $n=0.5$, incremental values of N_t cause a slight increase in microrotation profile, but for larger values of N_t, the profiles decline towards the freestream. **Figure 8(a)** and **Figure 8(b)** demonstrate impacts of N_t on temperature profiles when $n=0$ and $n=0.5$. **Figure 8(a)** illustrates that increasing the magnitude of N_t improves the temperature distribution when $n=0$. **Figure 8(b)** reveals that when $n=0.5$, there is an increase in the temperature profile within the region $0\le\eta\le 2.89$ as N_t increases.

Figures 9(a)-10(b) depict the effects of the gyrotactic microorganisms concentration difference parameter ς for various profiles when $n=0\&0.5$. In

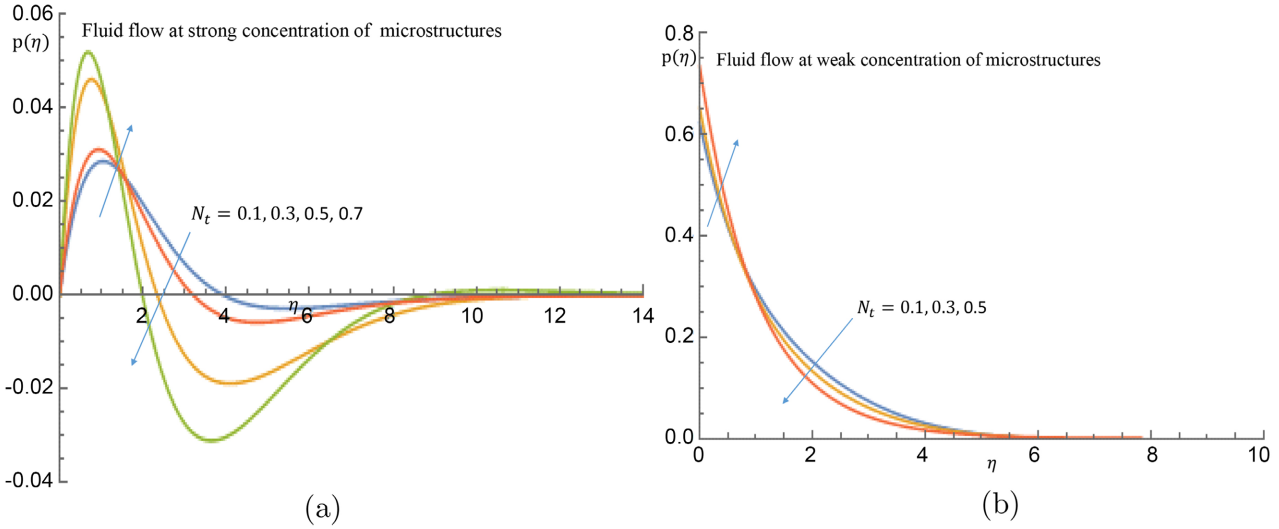

Figure 7. (a) Effect of N_t on microrotation profile when $n=0$; (b) effect of N_t on microrotation profile when $n=0.5$.

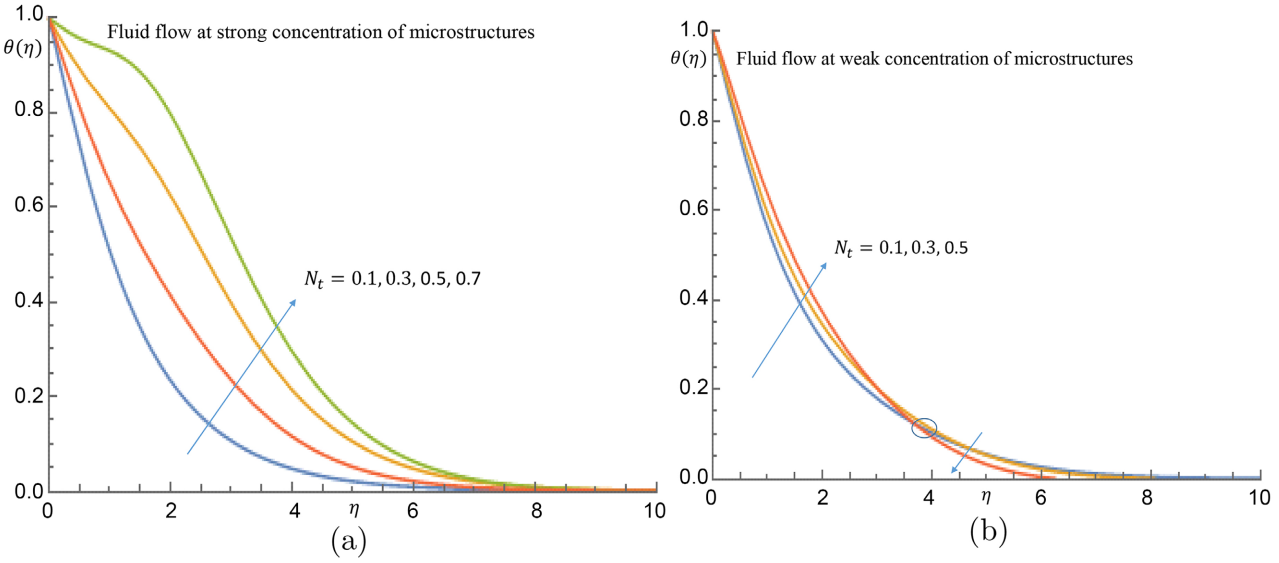

Figure 8. (a) Effect of N_t on temperature profile when $n=0$; (b) effect of N_t on temperature profile when $n=0.5$.

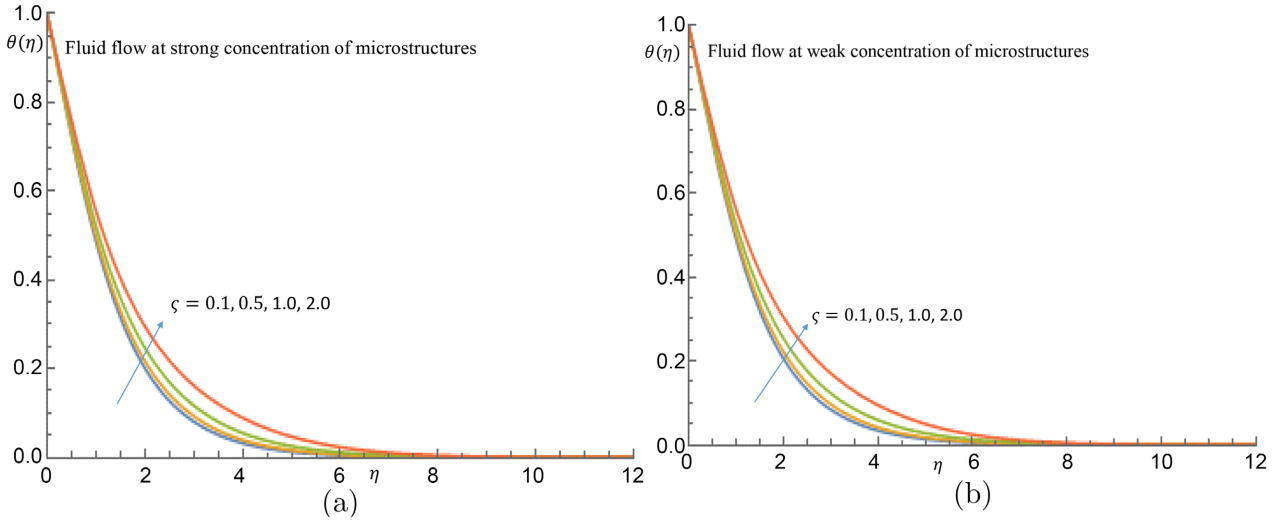

Figure 9. (a) Effect of ς on temperature profile when $n=0$; (b) effect of ς on temperature profile when $n=0.5$.

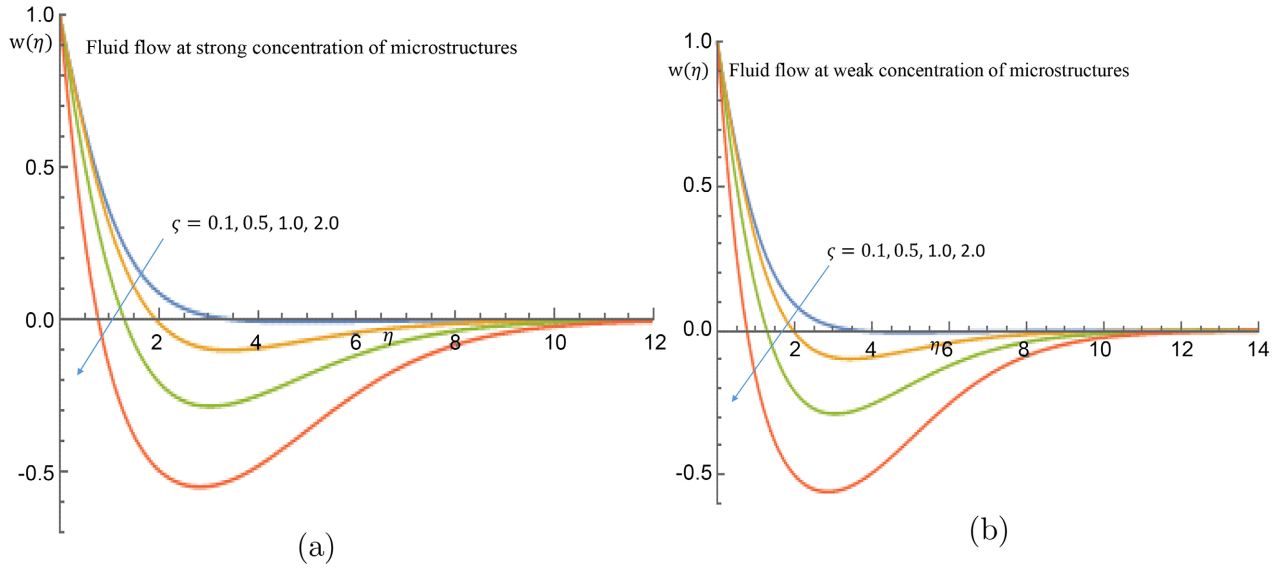

Figure 10. (a) Effect of ς on density of motile microorganisms profile when $n=0$; (b) effect of ς on density of motile microorganisms profile when $n=0.5$.

Figure 9(a) and **Figure 9(b)** when $n=0\&0.5$, incremental values of ς leads to temperature distribution augmentation. Physically, increasing the temperature of the fluid causes the bonds that hold the molecules of particles together to break down, allowing the microorganisms swimming within the fluid to interact and swim back to bottom layer of the fluid, allowing bioconvection to occur again. **Figure 10(a)** and **Figure 10(b)** indicate that increasing ς cause a noticeable reduction in the density of motile microorganisms profile for both $n=0\&0.5$.

5. Conclusions

In this communication, the influence of pertinent micropolar fluid flow para-

meters on nanoparticles and gyrotactic microorganisms is investigated. Both instances of strong and weak microelement concentrations are taken into consideration. The controlling flow equations were modeled and converted using suitable similarity variables. The series solution was determined using the Homotopy Analysis Method (HAM). The research produced the following important findings:

1) Incremental values of micropolar parameter K signifies enhancement of velocity profiles when $n=0$ & $n=0.5$, while the microrotation profiles increase when $n=0$ and declines when $n=0.5$.

2) Increasing values of micropolar parameter K corresponds to diminishing of temperature profiles when $n=0$ & $n=0.5$.

3) Incremental values of magnetic parameter M corresponds to decline of microrotation profile when $n=0$ while augmentation of microrotation is observed when $n=0.5$.

4) Temperature profiles are increasing functions of gyrotactic microorganisms concentration difference parameter ς for both $n=0$ & $n=0.5$, while density of motile microorganisms profiles are decreasing functions of ς for both $n=0$ & $n=0.5$.

Acknowledgements

The corresponding author "Dr. Tosin Oreyeni" would like to express his sincere appreciations to the respected reviewers for their technical and insightful comments that helped to enrich meaningfully the present investigation.

Conflicts of Interest

The authors declare no conflicts of interest regarding the publication of this paper.

References

[1] Platt, J.R. (1961) "Bioconvection Patterns" in Cultures of Free-Swimming. *Science*, **133**, 1766-1767. https://doi.org/10.1126/science.133.3466.1766

[2] Ghorai, S. and Hill, N.A. (2007) Gyrotactic Bioconvection in three Dimensions. *Physics of Fluids*, **19**, Article ID: 054107. https://doi.org/10.1063/1.2731793

[3] Raees, A., Xu, H., Sun, Q. and Pop, I. (2015) Mixed Convection in Gravity-Driven Nanoliquid Film Containing Both Nanoparticles and Gyrotactic Microorganisms. *Applied Mathematics and Mechanics*, **36**, 163-178. https://doi.org/10.1007/s10483-015-1901-7

[4] Waqas, H., Khan, S.A., Bhatti, M.M. and Hussain, S. (2021) Bioconvection Mechanism Using Third-Grade Nanofluid Flow with Cattaneo-Christov Heat Flux Model and Arrhenius Kinetics. *International Journal of Modern Physics B*, **35**, Article ID: 2150178. https://doi.org/10.1142/S0217979221501782

[5] Lv, Y.P., Gul, H., Ramzan, M., Chung, J.D. and Bilal, M. (2021) Bioconvective Reiner-Rivlin Nanofuid Fow over a Rotating Disk with Cattaneo-Christov Fow Heat Fux and Entropy Generation Analysis. *Scientific Reports*, **11**, Article No. 15859. https://doi.org/10.1038/s41598-021-95448-y

[6] Puneeth, V., Manjunatha, S. and Gireesha, B.J. (2021) Quartic Autocatalysis of Homogeneous and Heterogeneous Reactions in the Bioconvective Flow of Radiating Micropolar Nanofluid between Parallel Plates. *Heat Transfer*, **50**, 5925-5950. https://doi.org/10.1002/htj.22156

[7] Koriko, O.K., Shah, N.A., Saleem, S., Chung, J.D., Omowaye, A.J. and Oreyeni, T. (2021) Exploration of Bioconvection Flow of MHD Thixotropic Nanofluid Past a Vertical Surface Coexisting with Both Nanoparticles and Gyrotactic Microorganisms. *Scientific Reports*, **11**, Article No. 16627. https://doi.org/10.1038/s41598-021-96185-y

[8] Jawad, M., Saeed, A., Khan, A. and Islam, S. (2020) MHD Bioconvection Darcy-Forchheimer Flow of Casson Nanofluid over a Rotating Disk with Entropy Optimization. *Heat Transfer*, **50**, 2168-2196. https://doi.org/10.1002/htj.21973

[9] Eringen, A.C. (1966) Theory of Micropolar Fluids. *Journal of Mathematics and Mechanics*, **16**, 1-18. https://doi.org/10.1512/iumj.1967.16.16001

[10] Agarwal, V., Singh, B., Kumari, A., Jamshed, W., Nisar, K.S., Almaliki, A.H. and Zahran, H.Y. (2022) Steady Magnetohydrodynamic Micropolar Fluid Flow and Heat and Mass Transfer in Permeable Channel with Thermal Radiation. *Coatings*, **12**, Article No. 11. https://doi.org/10.3390/coatings12010011

[11] Mabood, F., Shamshuddin, M.D. and Mishra, S.R. (2022) Characteristics of Thermophoresis and Brownian Motion on Radiative Reactive Micropolar Fluid Flow towards Continuously Moving Flat Plate: HAM Solution. *Mathematics and Computers in Simulation*, **191**, 187-202. https://doi.org/10.1016/j.matcom.2021.08.004

[12] Ram, M.S., Shamshuddin, M.D. and Spandana, K. (2021) Numerical Simulation of Stagnation Point Flow in Magneto Micropolar Fluid over a Stretchable Surface under Influence of Activation Energy and Bilateral Reaction. *International Communications in Heat and Mass Transfer*, **129**, Article ID: 105679. https://doi.org/10.1016/j.icheatmasstransfer.2021.105679

[13] Kumar, K.A., Sugunamma, V. and Sandeep, N. (2019) Influence of Viscous Dissipation on MHD Flow of Micropolar Fluid over a Slendering Stretching Surface with Modified Heat Flux Model. *Journal of Thermal Analysis and Calorimetry*, **139**, 3661-3674. https://doi.org/10.1007/s10973-019-08694-8

[14] Kumar, K.A., Sugunamma, V. and Sandeep, N. (2019) Physical Aspects of Unsteady MHD Free Convective Stagnation Point Flow of Micropolar Fluid over a Stretching Surface. *Heat Transfer—Asian Research*, **48**, 3968-3985. https://doi.org/10.1002/htj.21577

[15] Koriko, O.K., Animasaun, I.L., Omowaye, A.J. and Oreyeni, T. (2019) The Combined Influence of Nonlinear Thermal Radiation and Thermal Stratification on the Dynamics of Micropolar Fluid along a Vertical Surface. *Multidiscipline Modeling in Materials and Structures*, **15**, 133-155. https://doi.org/10.1108/MMMS-12-2017-0155

[16] Koriko, O.K., Oreyeni, T., Omowaye, A.J. and Animasaun, I.L. (2016) Homotopy Analysis of MHD Free Convective Micropolar Fluid Flow along a Vertical Surface Embedded in Non-Darcian Thermally-Stratified Medium. *Open Journal of Fluid Dynamics*, **6**, 198-221. https://doi.org/10.4236/ojfd.2016.63016

[17] Choi, S.U.S. and Eastman, J.A. (1995) Enhancing Thermal Conductivity of Fluids with Nanoparticles. *Proceedings of* 1995 *ASME International Mechanical Engineering Congress and Exposition*, San Francisco, 12-17 November 1995, 99-105.

[18] Senthilraja, S., Karthikeyan, M. and Gangadevi, R. (2010) Nanofluid Applications in Future Automobiles: Comprehensive Review of Existing Data. *Nano-Micro Letters*,

2, 306-310. https://doi.org/10.1007/BF03353859

[19] Shah, N.A., Oreyeni, T., Shah, R., Salah, B. And Chung, J.D. (2021) Brownian Motion and Thermophoretic Diffusion Effects on the Dynamics of MHD Upper Convected Maxwell Nanofluid Flow Past a Vertical Surface. *Physica Scripta*, **96**, Article ID: 125722. https://doi.org/10.1088/1402-4896/ac36ea

[20] Amar, N. and Kishan, N. (2021) The Influence of Radiation on MHD Boundary Layer Flow Past a Nano Fluid Wedge Embedded in Porous Media. *Partial Differentiation Equations in Applied Mathematics*, **4**, Article ID: 100082. https://doi.org/10.1016/j.padiff.2021.100082

[21] Ghasemi, S.E. and Hatami, M. (2021) Solar Radiation Effects on MHD Stagnation Point Flow and Heat Transfer of a Nanofluid over a Stretching Sheet. *Case Studies in Thermal Engineering*, **25**, Article ID: 100898. https://doi.org/10.1016/j.csite.2021.100898

[22] Rasool, G. and Zhang, T. (2019) Characteristics of Chemical Reaction and Convective Boundary Conditions in Powell-Eyring Nanoflid Flow along a Radiative Riga Plate. *Heliyon*, **5**, e01497. https://doi.org/10.1016/j.heliyon.2019.e01479

[23] Fayyadh, M.M., Roslan, R., Kandasamy, R., Ali, I.R. and Hussein, N.A. (2019) Effect of Biot Number on Convective Heat Transfer of Darcy-Forchheimer Nanofluid Flow over Stretched Zero Mass Flux Surface in the Presence of Magnetic Field. *Journal of Advanced Research in Fluid Mechanics and Thermal Sciences*, **1**, 93-106.

[24] Nayak, M.K., Shaw, S., Makinde, O.D. and Chamkha, A.J. (2019) Investigation of Partial Slip and Viscous Dissipation Effects on the Radiative Tangent Hyperbolic Nanofluid Flow Past a Vertical Permeable Riga Plate with Internal Heating: Bungiorno Mode. *Journal of Nanofluids*, **8**, 51-62. https://doi.org/10.1166/jon.2019.1576

[25] Hayat, T., Shehzad, S.A. and Qasim, M. (2010) Mixed Convection Flow of a Micropolar Fluid with Radiation and Chemical Reaction. *International Journal for Numerical Methods in Fluids*, **67**, 1418-1436. https://doi.org/10.1002/fld.2424

[26] Saleem, S., Rafiq, H., Al-Qahtani, A., Abd El-Aziz, M., Malik, M.Y. and Animasaun, I.L. (2019) Magneto Jeffrey Nanofluid Bioconvection over a Rotating Vertical Cone Due to Gyrotactic Microorganism. *Mathematical Problems in Engineering*, **2019**, Article ID: 3478037. https://doi.org/10.1155/2019/3478037

[27] Liao, S.J. (2003) Beyond Perturbation: Introduction to the Homotopy Analysis Method. Chapman Hall/CRC Press, Boca Raton.

[28] Shah, N.A., Yook, S.J. and Oreyeni, T. (2022) Analytic Simulation of Thermophoretic Second Grade Fluid Flow Past a Vertical Surface with Varible Fluid Characteristics and Convective Heating. *Scientific Reports*, **12**, Article No. 5445. https://doi.org/10.1038/s41598-022-09301-x

[29] Oreyeni, T. and Omokhuale, E. (2019) Optimal Homotopy Analysis of MHD Natural Convection of Thermal Stratifcation: Boundary Layer Analysis. *American Journal of Computational Mathematics*, **9**, 116-131. https://doi.org/10.4236/ajcm.2019.92009

[30] Koriko, O.K., Oreyeni, T. and Oyem, O.A. (2018) On the Analysis of Variable Thermophysical Properties of Thermophoretic Viscoelastic Fluid Flow Past a Vertical Surface with n^{th} Order of Chemical Reaction. *Open Access Library Journal*, **5**, e4271. https://doi.org/10.4236/oalib.1104271

[31] Oreyeni, T., Omokhuale, E. and Sa'adu, L. (2017) The Effectiveness of Variable Properties on Thermophoresis Particle Deposition at the Levels of 1^{st} and 4^{th} Orders of Chemical Reaction of Buoyancy-Driven Flows of Second Grade Fluid. *International Journal of Science for Global Sustainability*, **4**, 67-82.